Synthetic and Systems Biotechnology 7 (2022) 460–473

Contents lists available at ScienceDirect

Synthetic and Systems Biotechnology

journal homepage: www.keaipublishing.com/en/journals/synthetic-and-systems-biotechnology

Original Research Article

Surface display of carbonic anhydrase on *Escherichia coli* for CO_2 capture and mineralization

Yinzhuang Zhu [a,1], Yaru Liu [a,1], Mingmei Ai [a], Xiaoqiang Jia [a,b,c,*]

[a] Department of Biochemical Engineering, School of Chemical Engineering and Technology, Tianjin University, Tianjin, 300072, PR China
[b] Frontier Science Center for Synthetic Biology and Key Laboratory of Systems Bioengineering (MOE), School of Chemical Engineering and Technology, Tianjin University, Tianjin, 300350, PR China
[c] Collaborative Innovation Center of Chemical Science and Engineering (Tianjin), Tianjin, 300072, PR China

ARTICLE INFO

Keywords:
Carbonic anhydrase
Cell surface display
Enzyme stability
CO_2 mineralization
Ice nucleation protein

ABSTRACT

Mineralization catalyzed by carbonic anhydrase (CA) is one of the most promising technologies for capturing CO_2. In this work, *Escherichia coli* BL21(DE3) was used as the host, and the *N*-terminus of ice nucleation protein (INPN) was used as the carrier protein. Different fusion patterns and vectors were used to construct CA surface display systems for α-carbonic anhydrase (HPCA) from *Helicobacter pylori* 26695 and α-carbonic anhydrase (SazCA) from *Sulfurihydrogenibium azorense*. The surface display system in which HPCA was fused with INPN via a flexible linker and intermediate repeat sequences showed higher whole-cell enzyme activity, while the enzyme activity of the SazCA expression system was significantly higher than that of the HPCA expression system. The pET22b vector with the signal peptide PelB was more suitable for the cell surface display of SazCA. Cell fractionation and western-blot analysis indicated that SazCA and INPN were successfully anchored on the cell's outer membrane as a fusion protein. The enzyme activity of the surface display strain E-22b-I_{RL}S (11.43 $U{\cdot}mL^{-1}OD_{600}{}^{-1}$) was significantly higher than that of the intracellular expression strain E-22b-S (8.355 $U{\cdot}mL^{-1}OD_{600}{}^{-1}$) under optimized induction conditions. Compared with free SazCA, E-22b-I_{RL}S had higher thermal and pH stability. The long-term stability of SazCA was also significantly improved by surface display. When the engineered strain and free enzyme were used for CO_2 mineralization, the amount of $CaCO_3$ deposition catalyzed by the strain E-22b-I_{RL}S on the surface (241 mg) was similar to that of the free SazCA and was significantly higher than the intracellular expression strain E-22b-S (173 mg). These results demonstrate that the SazCA surface display strain can serve as a whole-cell biocatalyst for CO_2 capture and mineralization.

1. Introduction

Carbon dioxide (CO_2) is the main greenhouse gas responsible for anthropogenic climate change [1]. Since the industrial revolution, large amounts of CO_2 emissions were generated due to the widespread use of fossil fuels and the global spread of large-scale industrial production. The continuous increase of CO_2 concentration has caused global warming, affecting the environment and human health [2]. The Kyoto and Paris agreements established the goals and responsibilities of all participating countries to jointly reduce CO_2 emissions in this century and limit the increase of the average global temperature to less than 2 °C [3,4]. Therefore, reducing CO_2 emissions and converting them into useable materials is of great significance for sustainable development. It is essential to develop a series of technologies that can reduce carbon dioxide emissions and capture them from the atmosphere. A series of technologies that can capture CO_2 have been developed, such as physical absorption [5–7], chemical absorption [8–10], cryogenic condensation [11], and membrane-based separation [12]. Although these methods can effectively capture CO_2, they also have problems such as the generation of by-products, high energy consumption, and secondary pollution [13,14]. The use of biological processes for carbon capture and storage (CCS) is an eco-friendly means to reduce the concentration of CO_2 in the atmosphere and reduce CO_2 emissions at the source, which can avoid the problem of secondary pollution during CO_2 capture. In

Peer review under responsibility of KeAi Communications Co., Ltd.

* Corresponding author. Department of Biochemical Engineering, School of Chemical Engineering and Technology, Tianjin University, Tianjin 300072, PR China.
E-mail address: xqjia@tju.edu.cn (X. Jia).

[1] These authors contributed equally to this work and should be considered co-first authors.

https://doi.org/10.1016/j.synbio.2021.11.008
Received 3 October 2021; Received in revised form 25 November 2021; Accepted 28 November 2021

addition to biological carbon fixation by higher plants, many microorganisms in nature can also capture CO_2, with well-known examples including species of *Xylella, Clostridium*, *Chlorella*, and *Rhodococcus* [15]. It is generally believed that algae are an ideal biological platform for CO_2 conversion, but algal cultivation faces challenges related to the careful selection of suitable species, controlling the light intensity, controlling the cell density, and oxygen accumulation [16,17].

Biological capture of CO_2 proceeds through a series of catalytic reactions. Carbonic anhydrase (CA; EC4.2.1.1) is widely distributed in the chloroplasts of plants and algae, where it plays a vital role in the fixation of CO_2 in photosynthesis [18]. Meldrum and Roughton first isolated carbonic anhydrase from bovine red blood cells, a metalloenzyme with Zn^{2+} as the active center [19]. It can efficiently catalyze the reversible hydration reaction $CO_2 + H_2O \leftrightharpoons HCO_3^- + H^+$. The catalytic rate of CA is 10^7 times higher than the spontaneous reaction rate under the same conditions, and it is one of the enzymes with the highest known catalytic rates [20]. CA has been used in industrial CO_2 capture due to its high catalytic activity, and its final product, $CaCO_3$, is very stable throughout the geological cycle and is environmentally friendly. Therefore, the use of CA for CO_2 mineralization has become one of the most promising CO_2 capture and utilization technologies [21].

The use of CA to capture CO_2 has attracted increasing attention due to its mild reaction conditions, lack of secondary pollution, and simplicity [22]. However, the use of isolated CA enzyme is limited by its high purification cost, poor stability, easy inactivation, and inability to recycle the biocatalyst. The use of whole-cell catalysts can effectively solve these problems, and many studies have confirmed that it is feasible to enhance the yield and improve the properties of an enzyme by modifying microorganisms to construct a whole-cell biocatalyst. At present, the technology for the intracellular microbial expression of CA is mature [23–25], but it still has significant shortcomings in practical applications. CO_2 and HCO_3^- are small molecules that can enter and exit cells freely, but the contact of intracellular CA with the substrate is still restricted to a large extent by the cell membrane. The timely discharge of products is also limited, thus reducing the catalytic efficiency of CA. Jo et al. expressed carbonic anhydrase derived from *Neisseria gonorrhoeae* (ngCA) in soluble form in the periplasmic space of *E. coli* BL21 (DE3). Compared with cytoplasmic expression, it showed a higher ability to hydrate CO_2 and accelerated calcium carbonate ($CaCO_3$) formation, but still had low activity due to the barrier effect of the outer membrane [26]. By contrast, if the enzyme is displayed on the cell surface, it is still protected by the cell to a certain extent, while allowing the substrate to directly contact the enzyme without passing through the membrane barrier, reducing the substrate and product mass transfer resistance, which greatly improves the enzymatic activity of the whole-cell catalyst.

In 1985, George P. Smith et al. invented cell surface display technology [27]. A specific protein or short peptide (target protein) and the outer membrane protein (carrier protein) of the microbial cell are anchored on the microbial cell surface in the form of a fusion protein through genetic engineering. *Escherichia coli* is one of the most popular host cells for producing recombinant proteins, and its expression platform is completely mature due to the availability of detailed genetic information, a wide-ranging genetic toolbox, and the ability to display full-length recombinant proteins on a high-density surface [28,29]. In 2011, Fan et al. used the ice nucleoprotein INPN to display HPCA on the surface of *E. coli* BL21(DE3) for the first time. The highest whole-cell enzyme activity reached 60.9 $mU{\cdot}mL^{-1}OD_{600}{}^{-1}$, and the results indicated that the HPCA displayed on the surface is more stable than free HPCA [30]. INPN has been proven suitable as a carrier protein to maximize the surface display of target proteins and increase the activity of displayed enzymes. In recent years, surface display systems including *E. coli*, *S. cerevisiae*, and *R. sphaeroides* have been developed to capture CO_2 using CA enzymes from different sources [2,26,31–34]. However, the whole-cell catalytic activity in these studies remained comparatively low. In addition to the catalytic activity of carbonic anhydrase itself, the main factors affecting the whole-cell catalytic activity are the fusion pattern of the target protein to the carrier, and the effect of different signal peptides on the transmembrane transfer of the target protein. The surface of *E. coli* was used to display α-carbonic anhydrase from *Sulfurihydrogenibium azorense* (SazCA) to achieve CO_2 capture, which has not been reported before.

In this work, *E. coli* BL21(DE3) was used as the host cell for the surface display of CA to construct a new whole-cell biocatalyst. INPN was used as the carrier protein, and was fused to HPCA in different patterns. Additionally, SazCA was displayed via the fusion of two sub-repeats and linkers in the middle repeat domain of ice nucleation protein in different vectors (pET-28a, pET-22b, and pET-32a). The various properties of the whole-cell catalyst displaying SazCA on its surface were further studied. Western blot analysis confirmed the localization of the fusion protein on the outer membrane of the host cell. The induction temperature, IPTG concentration, $ZnSO_4$ concentration, and induction duration were optimized to improve the whole-cell catalytic activity of the SazCA surface display strain and intracellular SazCA strain, which were then compared to assess the value of surface display. Additionally, we studied the effects of temperature, pH, metal ions, and long-term catalysis on the enzyme activity of the SazCA surface display strain and free SazCA enzyme. Finally, we used the whole-cell catalyst displaying SazCA on its surface for CO_2 mineralization, laying the foundation for the industrial application of this type of CA catalyst.

2. Materials and methods

2.1. Bacterial strains, plasmids, and culture conditions

All bacterial strains and plasmids used in this study are listed in Table 1. The construction and storage of recombinant plasmids were performed in *E. coli* DH5α (DSM6897). *E. coli* BL21 (DE3) (F^- ompT hsdS (r_B^-, m_B^-) gal dcm(DE3)) was used as a host strain for the surface display of carbonic anhydrase. The plasmid p2-inak harboring the partial gene sequences of INPN stored in our laboratory was used as template to amplify the *N*-terminal sequence of the carrier protein INP and the intermediate repetitive sequence (GenBank: PBP57058.1, **appendix A Sequence 1**). The sequences of *Helicobacter pylori* 26695 α-carbonic anhydrase (HPCA) (GenBank: MZ584769, **appendix A Sequence 2**) and *Sulfurihydrogenibium azorense* α-carbonic anhydrase (SazCA) (GenBank: MZ584770, **appendix A Sequence 3**) and codon-optimized for *E. coli* BL21(DE3) were synthesized by Genecreate (China). The plasmids pET-28a (+), pET-32a (+), and pET-22b (+) containing the T7 promoter were used for cloning and protein expression. Unless stated otherwise, all *E. coli* strains were grown in Luria–Bertani (LB) broth containing 5 g/L yeast extract, 10 g/L sodium chloride, and 10 g/L peptone, adjusted to a pH of 7.2–7.4. The initial culture temperature for all strains was 37 °C. Once the cultures reached the logarithmic growth phase (OD_{600} = 0.6–0.8), IPTG was added to induce protein expression (0.2 mM final concentration), which was continued at 25 °C for 10 h. At the same time, $ZnSO_4$ was added to increase CA activity (0.5 mM final concentration).

2.2. Plasmid construction

INPN was used as a carrier protein to display α-carbonic anhydrase from *Helicobacter pylori* 26695 (HPCA) [35] and α-carbonic anhydrase from *Sulfurihydrogenibium azorense* (SazCA) [36]. Fig. 1 shows the recombinant plasmids constructed in this work. INPN and HPCA were cloned into plasmid pET-28a in three fusion patterns to construct the HPCA surface display system, including the front two sub-repeats in the middle repeat domain of ice nucleoprotein (Re); linker (Flexible Linker, GGGGS); the front two sub-repeats in the middle repeat domain of ice nucleoprotein and linker. The primers for PCR cloning are listed in Table 2. The primers P1 and P2 were used to amplify the INPN-coding fragment, carrying the linker; the primers P1 and P3 were used to amplify the INPN-coding fragment and the Re-coding fragment; and the

Table 1
Strains and plasmids used in this work.

Name	Description	Source
Strains		
E. coli BL21 (DE3)	F⁻ ompT hsdS (r_B^-, m_B^-) gal dcm(DE3)	TransGen Biotech
E. coli DH5α	F⁻ φ80d *lac*ZΔM15Δ(*lac*ZYA-*arg*F)U169 *end*A1 *rec*A1 *hsdR*17 (r_k^-, m_k^+) *sup*E44λ-*thi*-1 *gyrA*96 *rel*A1 *pho*A	TransGen Biotech
E-28a	*E. coli* BL21(DE3) harboring empty vector pET-28a (+)	This study
E-22b	*E. coli* BL21(DE3) harboring empty vector pET-22b (+)	This study
E-32a	*E. coli* BL21(DE3) harboring empty vector pET-32a (+)	This study
E-28a-H	*E. coli* BL21(DE3) harboring p28a-H	This study
E-28a-I_LH	*E. coli* BL21(DE3) harboring p28a- I_LH	This study
E-28a-I_RH	*E. coli* BL21(DE3) harboring p28a- I_RH	This study
E-28a-I_{RL}H	*E. coli* BL21(DE3) harboring p28a- I_{RL}H	This study
E-22b-H	*E. coli* BL21(DE3) harboring p22b-H	This study
E-22b-I_{RL}H	*E. coli* BL21(DE3) harboring p22b-I_{RL}H	This study
E-32a-H	*E. coli* BL21(DE3) harboring p32a-H	This study
E-32a-I_{RL}H	*E. coli* BL21(DE3) harboring p32a-I_{RL}H	This study
E-28a-S	*E. coli* BL21(DE3) harboring p28a-S	This study
E-28a-I_{RL}S	*E. coli* BL21(DE3) harboring p28a-I_{RL}S	This study
E-22b-S	*E. coli* BL21(DE3) harboring p22b-S	This study
E-22b-I_{RL}S	*E. coli* BL21(DE3) harboring p22b-I_{RL}S	This study
E-32a-S	*E. coli* BL21(DE3) harboring p32a-S	This study
E-32a-I_{RL}S	*E. coli* BL21(DE3) harboring p32a-I_{RL}S	This study
Plasmids		
p2-inak	Harboring the partial gene sequences of INPN	Lab stock
pET-28a (+)	T7 promoter, parent vector for cloning and protein expression, Kan resistance	Lab stock
pET-22b (+)	T7 promoter, parent vector for the construction of surface display fusion genes, pelB signal sequence, Amp resistance	Lab stock
pET-32a (+)	T7 promoter, parent vector for the construction of surface display fusion genes, trxA thioredoxin sequence, Amp resistance	Lab stock
p28a-H	HPCA inserted into pET-28a	This study
p28a-I_LH	INPN-Linker-HPCA inserted into pET-28a	This study
p28a-I_RH	INPN (Re)-HPCA inserted into pET-28a	This study
p28a-I_{RL}H	INPN (Re)-Linker-HPCA inserted into pET-28a	This study
p22b-H	HPCA inserted into pET-22b fused with PelB signal peptide	This study
p22b-I_{RL}H	INPN (Re)-Linker-HPCA inserted into pET-22b fused with PelB signal peptide	This study
p32a-H	HPCA inserted into pET-32a fused with the solubility tag TrxA	This study
p32a-I_{RL}H	INPN (Re)-Linker-HPCA inserted into pET-32a fused with the solubility tag TrxA	This study
p28a-S	SazCA inserted into pET-28a	This study
p28a-I_{RL}S	INPN (Re)-Linker-SazCA inserted into pET-28a	This study
p22b-S	SazCA inserted into pET-22b fused with PelB signal peptide	This study
p22b-I_{RL}S	INPN (Re)-Linker-SazCA inserted into pET-22b fused with PelB signal peptide	This study
p32a-S	SazCA inserted into pET-32a fused with the solubility tag TrxA	This study
p32a-I_{RL}S	INPN (Re)-Linker-SazCA inserted into pET-32a fused with the solubility tag TrxA	This study

primers P1 and P4 were used to amplify the INPN-coding fragment that binds to the Re-coding fragment and linker. The p2-inak preserved in our laboratory was used as the template, and the resulting fragments were double-digested with *Nco*I/*Hind*III. The primers P6 and P7 were used to amplify the HPCA coding fragment, using p-HPCA as the template. The amplified HPCA coding fragment was double-digested with *Hind*III/*Xho*I. The INPN fusion protein fragments and the HPCA coding sequence were fused using T4 DNA ligase. The different fusion fragments were double-digested with *Nco*I/*Xho*I and inserted between the corresponding sites of pET-28a to generate the HPCA surface display vectors p28a-I_LH, p28a-I_RH, and p28a-I_{RL}H, respectively.

The α-carbonic anhydrase isolated from the extremophilic bacterium *Sulfurihydrogenibium azorense* (SazCA) in the Azores hot springs has the highest catalytic activity in the carbonic anhydrase family reported to date. Different vectors, including plasmid pET-28a, plasmid pET-22b with the PelB signal peptide, and plasmid pET-32b with the thioredoxin solubility tag (TrxA), were used to construct different HPCA and SazCA fusion proteins. The primers P5 and P7 were used to amplify the HPCA coding fragment, using p-HPCA as the template. Similarly, the primers P8 and P10 were used to amplify the SazCA coding fragment, using p-SazCA as the template. The amplified HPCA coding fragment and the amplified SazCA coding fragment were double-digested with *Nco*I/*Xho*I and inserted between the corresponding sites of pET-28a, pET-22b, and pET-32a to generate the intracellular HPCA expression vectors p28a-H, p22b-H, and p32a-H, as well as the intracellular SazCA expression vectors p28a-S, p22b-S, and p32a-S, respectively. The HPCA surface display vectors p22b-I_{RL}H and p32a-I_{RL}H were constructed analogously to the construction of p28a-I_{RL}H described above. To construct a fusion protein, INPN and SazCA were connected by the fusion of the front two sub-repeats in the middle repeat domain of ice nucleation protein and linker, and the fusion fragment was double-digested with *Nco*I/*Hind*III. The primers P9 and P10 were used to amplify the SazCA coding fragment, using p-SazCA as a template, and the amplified SazCA coding fragment was double-digested with *Hind*III/*Xho*I. The INPN fusion protein fragment and the SazCA coding sequence were fused using T4 DNA ligase. The fusion fragments were double-digested with *Nco*I/*Xho*I, and inserted between the corresponding sites of pET-28a, pET-22b, and pET-32a to generate the SazCA surface display vectors p28a-I_{RL}S, p22b-I_{RL}S, and p32a-I_{RL}S, respectively. All restriction enzymes were purchased from TransGen Biotech Co., Ltd (China). Plasmid extraction kits, PCR product purification kits, and agarose gel recovery kits were purchased from BioMed Biotech Co., Ltd (China).

2.3. Cell culture, protein expression and characterization

First, the recombinant strains were cultured overnight in 3 mL of LB medium at 220 rpm and 37 °C to reactivate the cryopreserved cells. Then, 2 mL of the resulting seed culture was used to inoculate a 250 mL Erlenmeyer flask containing 100 mL of LB medium and cultured at 37 °C and 220 rpm. When the OD_{600} reached 0.6–0.8, fresh LB medium was used to adjust the medium $OD_{600} = 0.6 \pm 0.02$, IPTG was added to induce protein expression (0–1.0 mM final concentration), which was continued at 15–37 °C for 6–60 h. At the same time, $ZnSO_4$ was added to increase CA activity (0–2.0 mM final concentration). Then, the cells were harvested by centrifugation at 7000 rpm and 4 °C for 10 min, washed twice with deionized water, washed twice with 0.02 M Tris-HCl buffer (pH 8.3), and resuspended in 10 mL of the same buffer. The OD_{600} was measured and the cell suspensions were stored at 4 °C for enzyme activity assay. All experiments were performed in triplicates.

2.3.1. Carbonic anhydrase enzyme activity assay

CA activity was determined using a classical electrochemical method [37]. Briefly, a sample comprising 200 μL of the mixed whole-cell catalyst was added to 10 mL of Tris-HCl buffer (0.02 M, pH = 8.3) on ice. After the pH electrode reading stabilized, 5 mL of ice-cold CO_2 saturated aqueous solution, and the pH change was recorded. The time taken for 8.3 to decrease to 6.3 is recorded as t, the blank control is combined with an equal volume of Tris-HCl buffer, and the empty control reaction time is recorded as t_0. Then the CA activity is calculated using the formula $U=(t_0-t)/t$, which gives the Wilbur-Anderson units (WAU), and expressed as the unit's enzyme activity per milliliter unit cell density ($U \cdot ml^{-1}OD_{600}^{-1}$). The entire test process is carried out in an ice bath.

2.3.2. Whole-cell immunofluorescence analysis

Immunofluorescence microscopy experiments were performed on the recombinant strains using a previously published method [30]. After the strains with different plasmids were induced to express the different fusion proteins for 12 h, the cells were collected by centrifugation,

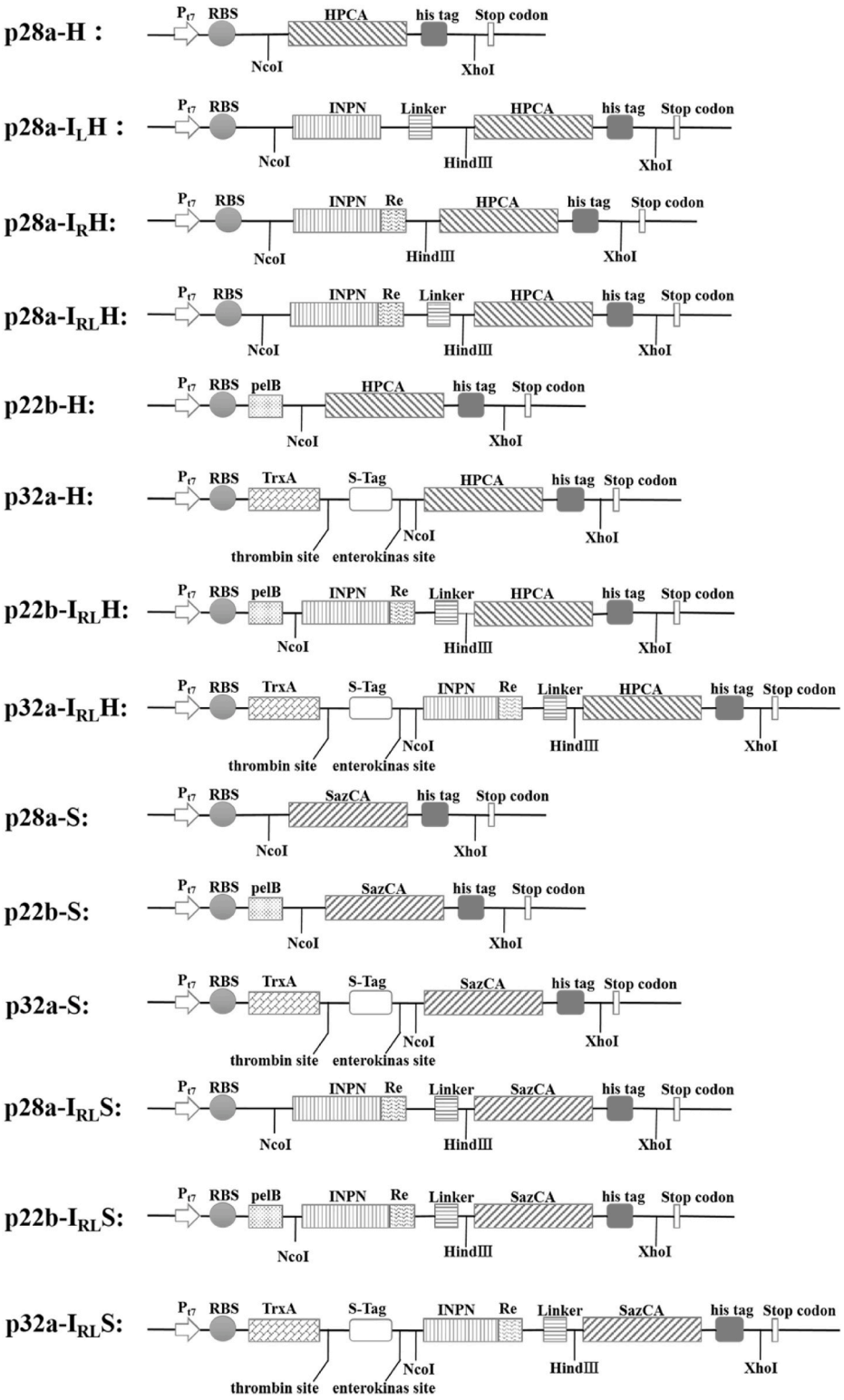

Fig. 1. Structure map of the recombined plasmids constructed in this study (Acronyms: INPN, *N*-domain of ice-nucleation protein; HPCA, α-carbonic anhydrase from *Helicobacter pylori* 26695; SazCA, α-carbonic anhydrase from *Sulfurihydrogenibium azorense*; Re, the front two sub-repeats in the middle repeat domain of ice nucleoprotein; Linker, Flexible Linker, GGGGS; P_{t7}, T7 promoter; RBS, ribosome-binding site; PelB, signal peptide; TrxA, solubility tag; The (His)6-Tag sequence was added between the fusio n protein and the stop codon for immunohistochemical detection).

washed with PBS three times, and then suspended in PBS to an OD_{600} = 1.0. Aliquots comprising 1 mL of the bacterial solution were centrifuged, and whole-cell pellet was fixed in 4% paraformaldehyde (PFA). The cells were then smeared on a slide, left to stand for 10 min, and soaked in 5% (w/v) BSA for 1 h to block unspecific protein binding sites. The BSA buffer was blotted away from the slide using absorbent paper, the slide was rinsed with PBS, and washed on a side-swing shaker three times for 5 min each. The slides were then placed in a petri dish with moist paper, and the rabbit anti-His IgG primary antibody with a dilution of 1/1000 (in 1% BSA buffer) was added dropwise onto the slide, and incubated overnight at 4 °C. On the next day, PBS was added dropwise, the slides were placed on a side-swing shaker, and shaken three times for 5 min each. After removing the PBS, the mouse anti-IgG secondary antibody (H + L) double-labeled with fluorescence and horseradish peroxidase at a dilution of 1/200 (in 1% BSA buffer) was added dropwise onto the slide and incubated at room temperature for 1 h. Then, PBS was added

Table 2
Primers used for the construction of recombinant plasmids.

Primers[a]	Sequence (5'→3')	Restriction site
P1: NcoI-INPN-F	CATGCCATGGGCATGACCCTGGATAAAGCACTGG	*Nco*I
P2: H-lin-INPN-R	CCCAAGCTTCGAACCGCCACCGCCGGTCTGCAAATTCTGCGGCG	*Hin*dIII
P3: H-INPN(Re)-R	CCCAAGCTTAATTAGATCACTGTGGTTGC	*Hin*dIII
P4: H-lin-INPN(Re)-R	CCCAAGCTTGCTGCCACCACCACCAATC	*Hin*dIII
P5: NcoI-HPCA-F	CATGCCATGGAAAATACCAAATGGGATTATAAGAATAAAG	*Nco*I
P6: H-HPCA-F	CCCAAGCTTATGGAGAACACCAAGTGGG	*Hin*dIII
P7: Xh-HPCA-R	CCGCTCGAGATTAGTGGTGGTGGTGGTGGTGGCGGGTCTCAGCTGAGC	*Xho*I
P8: NcoI-SazCA-F	CATGCCATGGGCGTGGCCGAGGTCCACCACTGGTC	*Nco*I
P9: H-SazCA-F	CCCAAGCTTATGGCCGAGGTCCACCACTGGTC	*Hin*dIII
P10: Xh-SazCA-R	CCGCTCGAGTCAGTGGTGGTGGTGGTGGTGGTTGCTTTCCAGGATGTAGC	*Xho*I

[a] Restriction sites are shown in underline.

dropwise to the slide and shaken for 5 min. After repeating three times, the buffer was removed from the slide using absorbent paper, after which DAPI staining solution was added dropwise and incubated at room temperature for 15 min to counter-stain the nuclei. Finally, the cells were observed under a E200 fluorescence microscope (Nikon, China).

2.3.3. Measurement of outer membrane integrity

For outer membrane integrity analysis, the cells were collected by centrifugation, washed with PBS (pH = 7.4) three times, and then diluted with PBS containing 2 mM EDTA to an $OD_{600} = 1.0$ in a 96-well plate. The change of the absorbance at 595 nm due to cell lysis was analyzed in a microplate reader, and recorded every 30 min for 6 h.

2.4. Detection of carbonic anhydrase cell surface localization

2.4.1. Cell fractionation

To determine whether the fusion protein was successfully anchored on the outer cell membrane, cell fractionation was performed for subsequent protein detection. An ultrasonicator (JY92-IIN, Scientz, China) was used to lyse the whole-cell catalyst at a power setting of 35%, and the total working time was 15 min (on for 4 s, pause for 4 s). The lysate was centrifuged 8000 rpm and 4 °C for 10 min to remove cell debris. The cleared lysate was transferred to a Beckman ultracentrifuge tube, and centrifuged at 40,000 rpm for 1 h. The resulting supernatant contained the cytoplasmic fraction, and the pellet contained the membrane fraction. The pellet was resuspended in PBS containing 0.01 mM $MgCl_2$ and 2% TritonX-100, incubated at room temperature for 30 min, and then centrifuged at 40,000 rpm for 1 h. The resulting supernatant was the inner membrane fraction, and the pellet was the outer membrane fraction. Each fraction was analyzed by SDS-polyacrylamide gel electrophoresis (SDS-PAGE) and western blotting as described below.

2.4.2. SDS-PAGE

Samples comprising 20 μL of each fraction were combined with 5 μL of 5 × SDS buffer, mixed well, boiled in a water bath for 4 min, cooled to room temperature, centrifuged at 5000 rpm for 1 min, and the supernatant used as saple for SDS-PAGE analysis with 1 × MOPS electrophoresis buffer. After electrophoresis, ExBlue protein ultrafast staining solution was used to stain the gel. After staining, the staining solution was recovered, and the protein gel was observed under white light using a gel imager.

2.4.3. Western blot analysis

After SDS-PAGE, the protein bands were transferred to a polyvinylidene fluoride (PVDF) membrane using Bio-Rad wet transfer equipment. The blotted PVDF membrane was blocked with 5% skimmed milk for 1 h, and incubated overnight at 4 °C with the primary rabbit anti-His IgG antibody at a dilution of 1/1000. Then, the membrane was incubated for 1 h at room temperature with the rabbit anti-IgG secondary antibody conjugated with horseradish peroxidase (HRP) at a dilution of 1/200. After washing the membrane three times with TBST solution, it was developed using the chemiluminescence (ECL) detection kit.

2.5. Kinetic analysis and effective diffusivity coefficient calculation

The kinetic parameters and effective diffusion coefficient assay were based on the procedure described by Tan et al. [38]. The assay was based on monitoring pH variable time caused by the catalyzed conversion of different concentrations of CO_2 to bicarbonate. All of the data were fitted with the Michaelis-Menten model for calculation.

2.6. CO_2 mineralization

To compare the efficacy of the SazCA surface display strain E-22b-I_{RL}S, intracellular expression strain E-22b-S, and free SazCA in CO_2 mineralization, 1 mg of carbonic anhydrase or whole-cell catalyst was added to 8 mL of 0.02 M Tris-HCl buffer pH 8.3, followed by 50 mL of ice-cold CO_2-saturated aqueous solution. After 5 min of reaction, the cells were removed by centrifugation. Then 25 mL of $CaCl_2$ solution was added to the liquid, and the reaction was maintained at the required temperature for 10 min. The water-based filter membrane was dried in a vacuum drying oven for 24 h and the weight recorded as W_1. The $CaCO_3$ precipitate was removed by vacuum filtration and the filter paper with the precipitate was placed in the vacuum drying oven for 36 h. The weigh after drying was recorded as W_2. The actual mass of mineralized $CaCO_3$ was then calculated using the formula $W=W_2–W_1$.

3. Results

3.1. Construction of CA surface display vectors

To determine the optimal fusion pattern between INPN and CA, the pET28a plasmid was used to construct the HPCA surface display vectors p28a-I_LH, p28a-I_RH, and p28-I_{RL}H, respectively, and the intracellular HPCA expression vector p28a-H as control (Fig. 1). The whole-cell enzyme activity of the HPCA engineered strains is shown in Fig. 2a. The whole-cell enzyme activity of the intracellular expression strain E-28a-H was 0.934 $U{\cdot}mL^{-1}OD_{600}{}^{-1}$. Among the different fusion modes between INPN and HPCA, both the HPCA surface display strains E-28a-I_RH and E-28a-I_{RL}H, with the front two sub-repeats in the middle repeat domain of ice nucleoprotein added to the fusion protein, showed higher whole-cell enzyme activity than E-28-I_LH. The strain E-28-I_{RL}H, which has an intermediate repeat sequence and linker (flexible linker, GGGGS) between INPN and HPCA, showed the highest whole-cell enzyme activity. To further improve the whole-cell enzyme activity of HPCA surface display strains, the cassette with the optimal fusion pattern was used to replace the pET22b plasmid with the signal peptide pelB and the pET32a plasmid with the solubility tag TrxA to construct the HPCA surface display systems. The results of whole-cell enzyme activity determination for all HPCA engineered strains are shown in Fig. 2b.

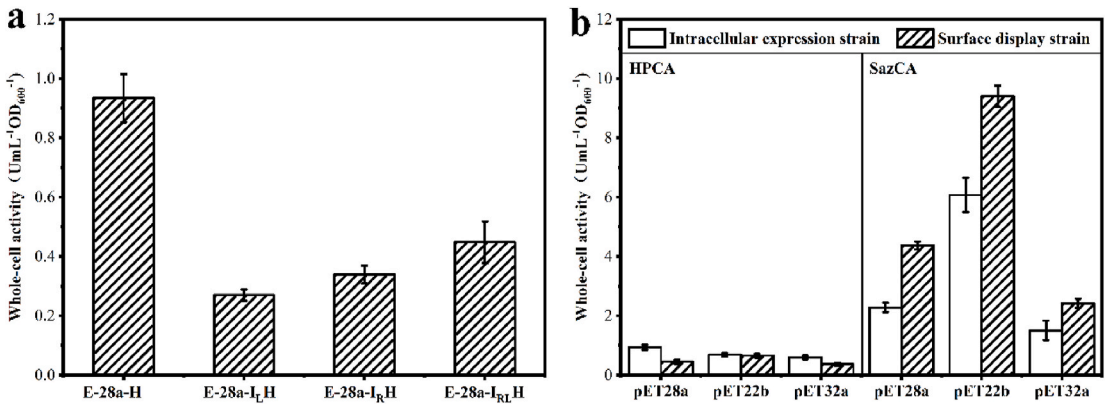

Fig. 2. Whole-cell enzyme activity of all CA expression strains. (a) Whole-cell enzyme activity of HPCA expression strains with different fusion patterns. (b) Whole-cell enzyme activity of CA expression strains with different vectors. The different CA expression strains are named according to the respective vector.

However, the whole-cell enzyme activity of the resulting HPCA display strains was not significantly improved, and the HPCA surface display strain E-22b-I_{RL}H exhibited the highest whole-cell enzyme activity of 0.652 U·mL^{-1}OD$_{600}$$^{-1}$. Although this was an improvement compared with the previous HPCA surface display system, the enzyme activity was still lower than that of the intracellular HPCA expression strain. Carbonic anhydrases from different sources appear to have different maximal whole-cell enzyme activity. In addition, the modification of the carrier structure and fusion pattern may also lead to unfavorable folding of HPCA, while the compatibility of HPCA with the surface display host cannot be ignored.

In this study, SazCA was displayed on the surface of *E. coli* BL21(DE3) for the first time. As shown in Fig. 1, the plasmids pET-28a without a tag, pET-22b with the pelB signal peptide, and pET-32a with the TrxA solubility tag were used to construct the SazCA surface display vectors p28a-I_{RL}S, p22b-I_{RL}S, and p32a-I_{RL}S, respectively, as well as the intracellular SazCA expression vectors p28a-S, p22b-S, and p32a-S as controls. INPN and SazCA were fused for surface display via two front-end sub-repeats in the middle repeat domain of ice nucleation protein and a linker. The results of whole-cell enzyme activity determination for all SazCA engineered strains are shown in Fig. 2b. The intracellular expression strain E-22b-S and the surface display strain E-22b-I_{RL}S constructed using the pET22b plasmid with the PelB signal peptide showed the highest whole-cell enzyme activity, which was similar to the HPCA surface display strains described above. The whole-cell enzyme activity of E-22b-I_{RL}S (9.402 U·mL^{-1}OD$_{600}$$^{-1}$) was significantly higher than that of E-22b-S (6.073 U·mL^{-1}OD$_{600}$$^{-1}$). In addition, CA from different sources can significantly improve the whole-cell activity of surface display strains. Compared with the strains expressing HPCA, the whole-cell activity of the strains expressing SazCA was dramatically increased, and the surface display strains showed an even more significant improvement (Fig. 2b). Therefore, as the CA with the highest catalytic activity reported to date, SazCA can greatly improve the whole-cell catalytic activity of surface display strains.

3.2. Detection of the cell surface localization and protein expression of SazCA

The expression of the target protein in the surface display and intracellular expression strains was analyzed by whole-cell immunofluorescence microscopy. The results are shown in Fig. S1. The fluorescence of the surface display strain was clearly visible after induction, and the amount of fluorescence was more robust than that of the intracellular expression strain. The cell fluorescence of the strain E-28a-I_{RL}S with CA displayed on the surface was weaker than that of E-22b-I_{RL}S and E-32a-I_{RL}S. To further assess the cell integrity of different engineered bacteria, *E. coli* BL21(DE3) was used as a control. The results are shown in Fig. S2. After EDTA treatment, the absorbance values of E-32a-S and E-32a-I_{RL}S were lower than that of *E. coli* BL21(DE3), while the other engineered strains did not show significant differences compared to the control. Therefore, the expression and surface display of SazCA in the engineered strains E-32a-S and E-32a-I_{RL}S had a particularly negative effect on the host strain. According to the whole-cell enzyme activity, whole-cell fluorescence microscopy, and cell integrity analysis, the surface display strain E-22b-I_{RL}S and intracellular expression strain E-22b-S with pET-22b with the pelB signal peptide exhibited the best performance.

To determine whether the carrier protein INPN and SazCA were successfully fused and anchored to the cell's outer membrane, cell fractionation was performed, followed by western blot analysis. After cell fractionation of E-22b-I_{RL}S, the cytoplasm, inner cell membrane, and outer cell membrane were analyzed by western blot (WB) analysis. The results are shown in Fig. 3a. The WB results revealed apparent bands larger than 50 kDa in the outer membrane fraction, which was consistent with the size of the INPN-SazCA fusion protein (52.59 kDa), indicating that the fusion protein was successfully expressed on the surface of the strain E-22b-I_{RL}S. To obtain free SazCA, E-22b-S was subjected to protein purification, and the purified protein was analyzed by SDS-PAGE. As shown in Fig. 3b, the protein bands were located between 22 and 30 kDa, which was consistent with the theoretical size of SazCA of 27 kDa. There were almost no other contaminating protein bands. The concentration of purified protein was 0.6 mg/mL according to spectrophotometric analysis.

3.3. SazCA enzyme activity of whole-cell catalysts produced under different induction conditions

The primary purpose of the constructed genetically engineered strains was to obtain a large amount of the target protein. Due to differences between the expressed gene constructs, the optimal conditions for protein expression are different, even in the same host strain. As can be seen based on the growth curves of recombinant and wild-type bacteria (Fig. S3), the surface display of CA did not adversely affect the growth of the engineered strain E-22b-I_{RL}S. However, the addition of inducer IPTG and $ZnSO_4$ may have exerted pressure on strains other than E-22b-I_{RL}S. Therefore, we optimized the induction conditions (induction temperature, IPTG concentration, $ZnSO_4$ concentration, and induction duration) of the SazCA surface display strain E-22b-I_{RL}S and intracellular expression strain E-22b-S to compare their whole-cell catalytic activity under their respective optimal expression conditions. Before inducing protein expression, the strain was cultured at 37 °C to the logarithmic phase. Although 37 °C is the optimal growth temperature for *E. coli*, heterologous protein expression is commonly carried out at a lower temperatures because low temperature helps the protein fold

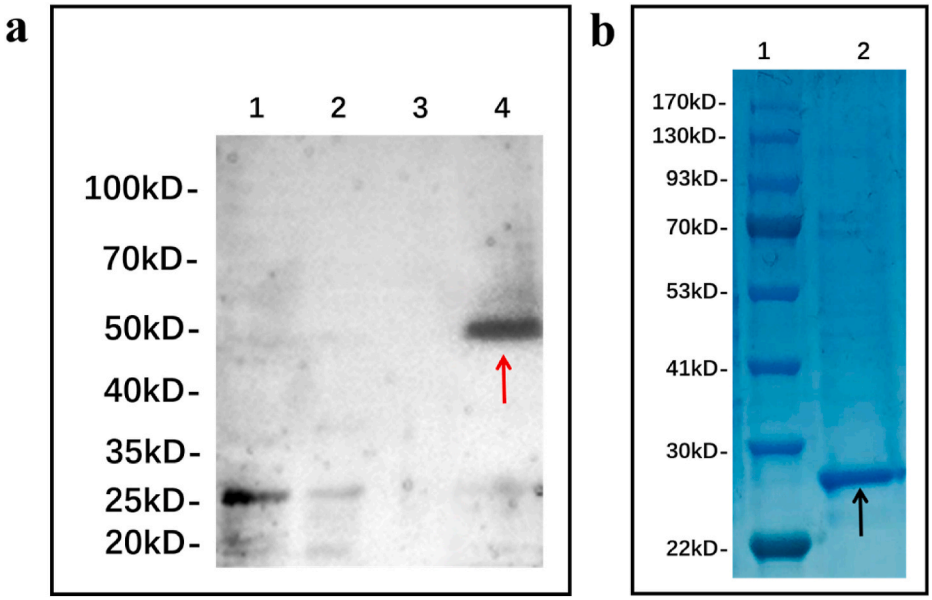

Fig. 3. (a) Western blot analysis of E-22b-I_{RL}S. The whole cell lysate of the *E. coli* BL21(DE3) containing pET22b was used as a blank control (lane 1), the cytoplasmic fraction (lane 2), inner cell membrane fraction (lane 3), and outer cell membrane fraction (lane 4). (b) SDS-PAGE of free SazCA purified from E-22b-S. Marker (lane 1), free SazCA (lane 2).

correctly and effectively [30]. Therefore, the strains E-22b-S and E-22b-I_{RL}S were induced to express the heterologous protein at 15 °C, 20 °C, 25 °C, 30 °C, and 37 °C respectively, and the results of whole-cell enzyme activity are shown in Fig. 4a. E-22b-S and E-22b-I_{RL}S had the highest whole-cell enzyme activity when induced at 25 °C, and the difference was statistically significant. However, the protein expression was reduced at 15 and 20 °C (Fig. S4), so the whole-cell enzyme activity was lower. When induced at 30 and 37 °C, it could be a considerable

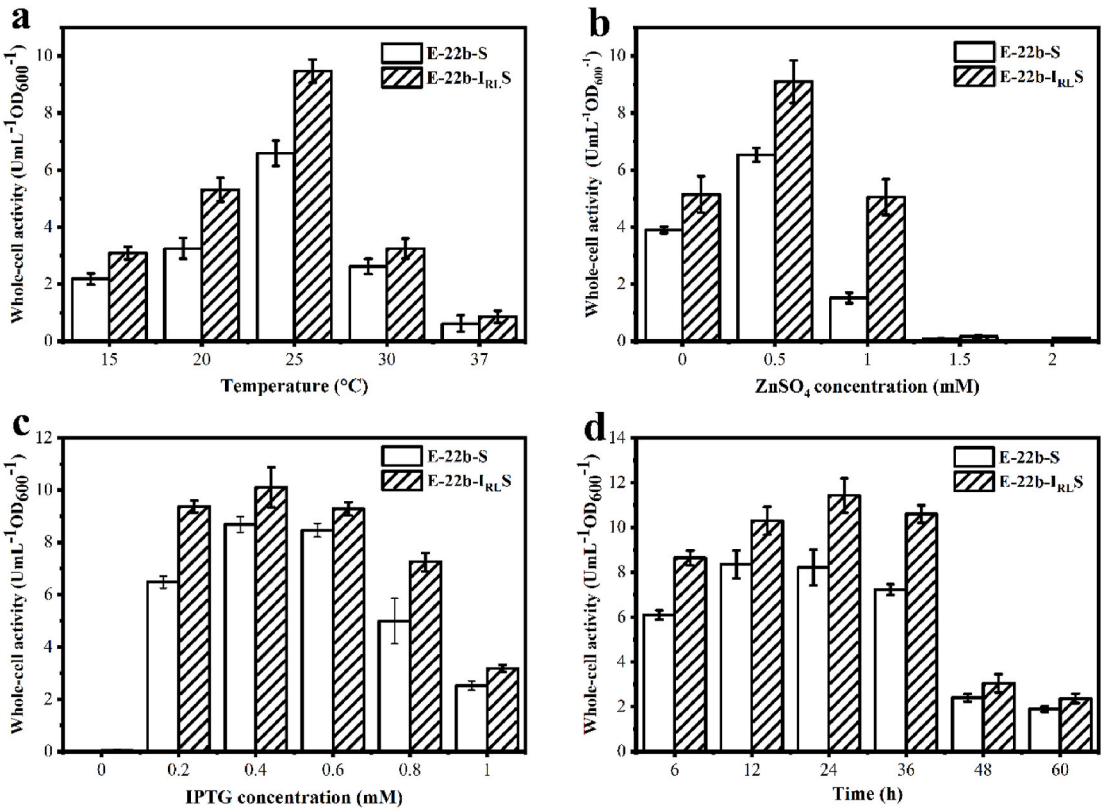

Fig. 4. Whole-cell SazCA enzyme activity under different induction conditions. The compared strains include the SazCA cell surface display strain E-22b-I_{RL}S and intracellular expression strain E-22b-S. (a) Induction temperature were set to 15, 20, 25, 30 and 37 °C, respectively, and the induction was performed for 12 h with the addition of 0.2 mM IPTG and 0.5 mM ZnSO4; (b) $ZnSO_4$ concentrations were set at 0, 0.5, 1.0, 1.5 and 2.0 mM, respectively, and 0.2 mM IPTG was added for induction at 25 °C for 12 h; (c) IPTG concentrations were set at 0, 0.2, 0.4, 0.6, 0.8 and 1.0 mM, respectively, and 0.5 mM $ZnSO_4$ was added for induction at 25 °C for 12 h; (d) Induction time were set to 6, 12, 24, 36, 48 and 60 h, respectively, and 0.4 mM IPTG and 0.5 mM $ZnSO_4$ were added for induction at 25 °C.

protein misfolding [39], resulting in the inactivity of the expressed protein.

Since carbonic anhydrase is a metalloenzyme with Zn^{2+} as the active center [19], during the induction of the engineered strains E-22b-S and E-22b-I_{RL}S, $ZnSO_4$ was added at final concentrations of 0 mM, 0.5 mM, 1.0 mM, 1.5 mM, and 2.0 mM. The results of whole-cell enzyme activity are shown in Fig. 4b. E-22b-S and E-22b-I_{RL}S showed a similar change trend of enzyme activity. Without additional Zn^{2+} beyond what is available in the LB medium, there was limited protein expression. When 0.5 mM Zn^{2+} was added to the medium, the enzyme activities of E-22b-S and E-22b-I_{RL}S were significantly increased to 6.538 and 9.101 $U{\cdot}mL^{-1}OD_{600}{}^{-1}$, respectively. However, when more than 0.5 mM Zn^{2+} was added, the whole-cell enzyme activity of E-22b-S and E-22b-I_{RL}S strains rapidly decreased. The SDS-PAGE analysis (Fig. S5) indicated that there was nearly no protein expression at the higher Zn^{2+} concentrations. As a well-known active agent [40], Zn^{2+} contributes to the large-scale expression of proteins in engineered bacteria. A small amount of Zn^{2+} from outside sources can help improve the strain's whole-cell CA activity. However, when the concentration of exogenously added Zn^{2+} is too high, it may have a strong negative effect on the host strain's growth and protein synthesis.

The T7-lac promoter was used to express the heterologous proteins in strains E-22b-S and E-22b-I_{RL}S following induction with IPTG. The concentration of the inducer IPTG is a significant factor affecting protein expression [41]. In theory, the expression level of the protein should be proportional to the IPTG concentration. However, IPTG also has potential toxicity to the host bacteria, and when the IPTG concentration is too high, the protein expression rate is too high, which will harm the transmembrane positioning of the protein being expressed, causing the protein to misfold and aggregate. In this case, the protein is more likely to form inclusion bodies, and at the same time, it will inhibit the growth of host cells [26]. The IPTG induction concentration of strains E-22b-S and E-22b-I_{RL}S was optimized, and the effects of inducer concentration on whole-cell enzyme activity are shown in Fig. 4c. In the absence of IPTG induction, neither strain E-22b-S nor E-22b-I_{RL}S showed detectable enzyme activity, and there was no prominent protein band in the SDS-PAGE gels. E-22b-I_{RL}S had the highest enzymatic activity when induced with 0.4 mM IPTG, and the enzyme activity was similar with 0.2 and 0.6 mM IPTG. When the IPTG concentration was increased to 0.8 mM and 1.0 mM, the enzyme activity significantly decreased. At IPTG concentrations between 0.2 and 1.0 mM, there was no significant difference in the protein expression level of E-22b-I_{RL}S (Fig. S6), indicating that at 0.6–1.0 mM IPTG, part of the protein may form inclusion bodies, resulting in a decrease of the whole-cell enzyme activity in spite of similar protein levels. The intracellular expression strain E-22b-S showed a similar change trend to that of E-22b-I_{RL}S.

To study the effect of induction time on the protein expression level, the engineered strains E-22b-S and E-22b-I_{RL}S were cultured at 37 °C to the logarithmic phase under the same conditions, and the induction time was set to 6 h, 12 h, 24 h, 36 h, 48 h, and 60 h. The results of whole-cell enzyme activity and protein expression are shown in Fig. 4d and Fig. S7. The intracellular expression strain E-22b-S showed the highest whole-cell enzyme activity and the highest protein expression after induction for 12 h. The surface display strain E-22b-I_{RL}S showed the highest whole-cell enzyme activity and the highest protein expression after 24 h of induction. These results revealed that the protein expression time also significantly impacted the final protein concentration and enzyme activity. If the induction time was too short, the engineered bacteria did not reach the plateau, and the total amount of cells did not reach the highest value, so that the induced protein expression was also reduced. However, if the induction time is too long, it will cause a part of the expressed protein to be degraded. Therefore, the engineered strains E-22b-S and E-22b-I_{RL}S were collected at 12 and 24 h after induction to prepare a whole-cell catalyst, respectively. Surface display strains require a longer induction time than intracellular expression strains because the transmembrane expression and localization of proteins are generally slower than intracellular expression.

In summary, the optimal induction temperature for E-22b-I_{RL}S and E-22b-S was 25 °C, the optimal IPTG concentration was 0.4 mM, the optimal Zn^{2+} concentration was 0.5 mM, and the optimal induction time was 24 and 12 h, respectively. Under their respective optimal induction conditions, the enzyme activity of the surface display strain E-22b-I_{RL}S (11.43 $U{\cdot}mL^{-1}OD_{600}{}^{-1}$) was significantly higher than that of the intracellular expression strain E-22b-S (8.355 $U{\cdot}mL^{-1}OD_{600}{}^{-1}$). It was further confirmed that carbonic anhydrase was displayed on the cell surface by genetic engineering to construct a new type of whole-cell biocatalyst that retains the enzyme's metabolic potential in the cell. It allows the substrate to directly contact the enzyme without passing through the membrane barrier, reducing the mass transfer resistance of the substrate and improving the catalyst's whole-cell enzyme activity.

3.4. Analysis of thermal stability

The thermal stability of enzymes is one of the most critical factors in industrial applications, so we studied the stability of E-22b-S, E-22b-I_{RL}S, and free SazCA at 25, 50 and 70 °C. As shown in Fig. 5a, the relative residual enzyme activities of E-22b-S, E-22b-I_{RL}S, and free SazCA remained almost constant at 25 °C, reaching 90.59, 95.05, and 83.23% of the initial enzyme activity after 12 h, respectively. By contrast, the enzyme activity of free SazCA decreased significantly faster with the extension of incubation time at 50 and 70 °C. After 12 h of incubation at 50 °C, the remaining relative enzyme activities of E-22b-S and E-22b-I_{RL}S were relatively close to 72%, while that of free SazCA dropped to 43.75% (Fig. 5b). After 12 h of incubation at 70 °C, the remaining enzyme activity of E-22b-I_{RL}S was close to 40%, while that of E-22b-S and free SazCA decreased to 29.11 and 15.12%, respectively (Fig. 5c). At present, CO_2 capture is mainly performed in post-combustion systems. As the CO_2 concentration in the flue gas of the post-combustion system is higher, it is more conducive to carbon capture and storage. However, the flue temperature is too high (about 140 °C), and the maximum temperature of CO_2 captured after cooling, and combustion is about 60 °C [42]. Therefore, the enzymes used for carbon capture must be thermostable. The crystal structures of the two carbonic anhydrases involved in this study have been determined and analyzed [35,36]. SazCA has an excellent heat resistance and can retain the hydration activity of carbon dioxide at high temperatures [36,43]. Furthermore, when SazCA is anchored on the surface of the outer membrane, the phospholipid environment of the membrane can protect the enzyme from thermal inactivation to a certain extent [44]. At the same time, the increase in hydrophobic amino acids caused by INPN will also increase the thermal stability of the fusion protein [45]. Therefore, the surface display of SazCA significantly improves its thermal stability and is expected to play an essential role in industrial applications. However, after increasing the temperature above the optimum value, the denaturation of *E. coli* proteins and the precipitation of cells will inevitably begin. The cell membrane structure will be destroyed, leading to the destruction of membrane integrity [46], which will affect the target display enzyme connected to the outer membrane.

3.5. Analysis of pH stability and long-term stability

The pH stability is also critical in CO_2 biomineralization because a large amount of CO_2 is absorbed in water, and the pH of the mineralization system will change due to the enzymatic reaction. From the perspective of the enzyme itself, the main effect of pH is on the enzyme's active region, which is composed of ionized groups. Proper ionization is needed to maintain the active conformation, facilitating substrate binding and catalysis [38]. To compare the effect of pH on the stability of E-22b-S, E-22b-I_{RL}S, and free SazCA, samples were incubated at 4 °C for 24 h in buffers with different pH values (citric acid-sodium citrate buffer at pH 4.0–6.0, Tris-HCl buffer at pH 7.0–9.0, and glycine-NaOH buffer at pH 10.0–12.0). The enzyme activity was measured in

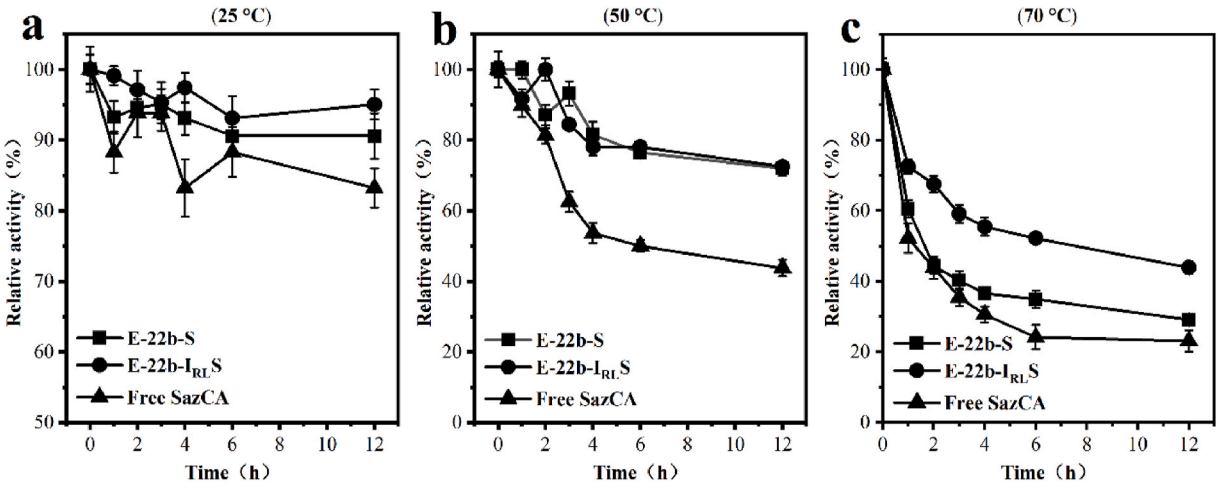

Fig. 5. The thermal stability of E-22b-S, E-22b-I$_{RL}$S, and free SazCA at different temperatures. Samples of E-22b-S, E-22b-I$_{RL}$S, and free SazCA were incubated in a water bath at 25, 50, and 70 °C for 0, 1, 2, 3, 4, 6, and 12 h. CO_2 was used as the substrate to measure the enzyme activity of different samples, and the enzyme activity at 0 h was defined as 100% calculate the residual enzyme activity of different samples at different temperatures. All data represent the averages of three independent measurements.

Tris-HCl at pH 8.3, and the maximal enzyme activity was defined as 100%. As shown in Fig. 6a, the relative enzyme activities of E-22b-S, E-22b-I$_{RL}$S, and free SazCA increased first and then decreased with increasing pH. Both showed the highest enzyme activity after incubation under alkaline conditions of pH = 9.0. At this pH, there was no significant difference in stability between the whole-cell biocatalyst and the free enzyme. Under acidic and strongly alkaline conditions, the surface display strain E-22b-I$_{RL}$S exhibits higher pH stability than E-22b-S and free SazCA. The process of CO_2 biomineralization is pH-dependent, and the solubility of carbonate increases at acidic pH [47]. However, carbonate precipitation must be carried out under alkaline conditions. Therefore, the increased pH stability of SazCA after surface display makes it more competitive for industrial applications. To compare the long-term stability of E-22b-S, E-22b-I$_{RL}$S and free SazCA, samples were incubated at 25 °C in the presence of CO_2 as a substrate for 0–10 d. As shown in Fig. 6b, the remaining enzyme activity of E-22b-I$_{RL}$S after ten days about 75% of the initial value, while the E-22b-S and free SazCA retained only 43.9 and 36.3% of the initial activity. The results therefore showed that the enzyme's long-term storage stability was significantly improved by anchoring it to the bacterial membrane.

3.6. Influence of metal ions on the stability of carbonic anhydrase

The active site of SazCA has a specific hydrophobic pocket responsible for the binding of CO_2 [48] which also participates in proton shuttling between the hydroxyl molecule bound to the metal ion and its surrounding environment [49]. To compare the effects of fourteen metal ions on the SazCA surface display strain E-22b-I$_{RL}$S and free SazCA, we

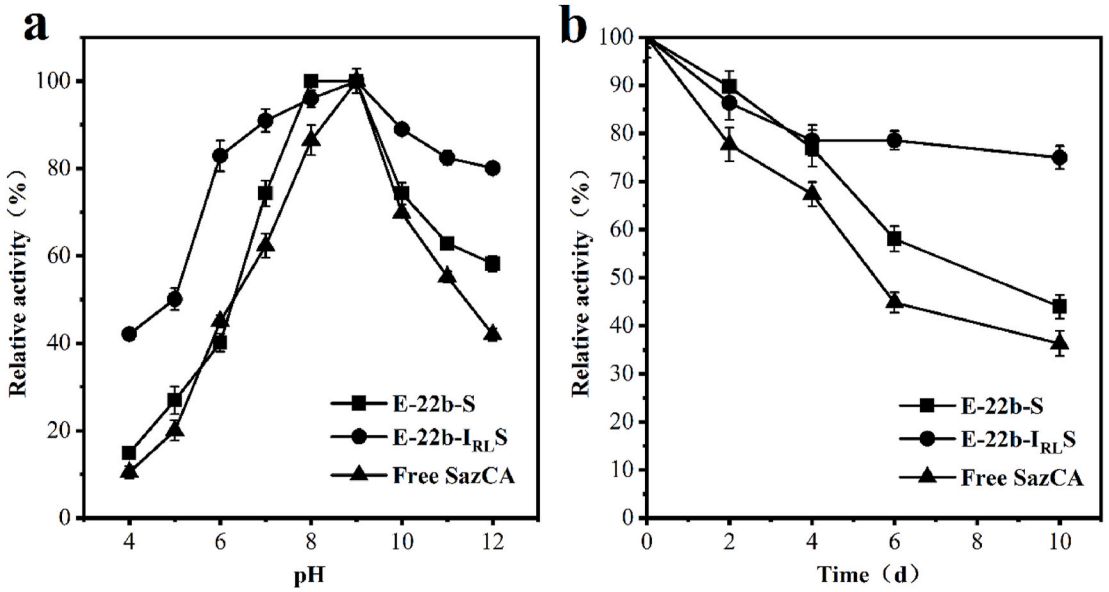

Fig. 6. (a) The pH stability of E-22b-S, E-22b-I$_{RL}$S, and free SazCA. E-22b-S, E-22b-I$_{RL}$S cells, and free SazCA enzyme were incubated at 4 °C for 24 h in buffers with different pH (citric acid-sodium citrate buffer at pH 4.0–6.0, Tris-HCl buffer at pH 7.0–9.0, and glycine-NaOH buffer at pH 10.0–12.0). The enzyme activity was measured in Tris-HCl at pH 8.3, and the maximal enzyme activity was defined at 100%. The data represent the means of three independent measurements. (b) The long-term stability of E-22b-I$_{RL}$S and Free SazCA. Samples of E-22b-I$_{RL}$S and free SazCA were incubated at 25 °C with CO_2 as the substrate. At the indicated time-points (0, 2, 4, 6, and 10 d) samples were taken to determine the residual enzyme activity. The enzyme activity measured at 0 d was defined as 100% and calculate the residual enzyme activity over time. The data represent the averages of three independent experiments.

added fourteen metal ions with a final concentration of 1.0 mM to the enzymatic reaction system, after which CO_2 was used as the substrate to measure the enzyme activity. The enzyme activity was measured at 0 °C in Tris-HCl buffer at pH 8.3. The enzyme activity without added metal ions was defined as 100%. As shown in Table 3, K^+, Na^+, Ca^{2+}, Fe^{3+}, and Mg^{2+} did not significantly affect the activity of E-22b-I_{RL}S and free SazCA, which remained above 80% in all cases. Fe^{3+} significantly increased the activity of E-22b-I_{RL}S and free SazCA, while Mg^{2+} increased the enzymatic activity of E-22b-I_{RL}S without having an effect on free SazCA. By contrast, Li^+, Mn^{2+}, Cu^{2+}, Ni^{2+}, As^{3+}, Hg^{2+}, Pb^{2+}, Cd^{2+}, and Zn^{2+} inhibited the enzyme activity of E-22b-I_{RL}S and free SazCA to various extents. This was especially true for Cu^{2+}, Cd^{2+}, and Zn^{2+}, which exhibited significant inhibitory effects. Studies have confirmed that mercury and lead ions, which are found in flue gases, are effective enzyme inhibitors [50]. Carbonic anhydrase is a metalloenzyme with Zn^{2+} in its active center. The addition of 0.5 mM $ZnSO_4$ during the process of inducing protein expression improved the expression of SazCA. Therefore, we further explored the effect of Zn^{2+} on enzyme activity. The final concentration of Zn^{2+} in the enzymatic reaction system was set to 0 mM, 0.5 mM, 1.0 mM, 1.5 mM, 2.0 mM after which the enzyme activity E-22b-I_{RL}S and free SazCA was measured as shown in Table 3. When the concentration of Zn^{2+} was set to 0.5 mM, the inhibitory effect on enzyme activity was weak, but at 1.0 mM Zn^{2+}, the inhibitory effect was noticeable. When the concentration of Zn^{2+} was increased to 1.5 and 2.0 mM, the enzyme was completely inhibited. An early study found that although CA is a zinc-dependent enzyme, its tightly bound form of Zn^{2+} accounts for only 0.3% (equivalent to 0.046 mM) [51]. However, if other transition metals (Mn^{2+}, Co^{2+}, Cu^{2+}, and Zn^{2+}) or higher concentrations were added to the system, they could form complexes and reduce enzyme activity.

3.7. Kinetic analysis of whole-cell biocatalyst

Studying the kinetic parameters of whole-cell biocatalysts is critical for their evaluation and biocatalysis applications. According to the method used by Tan et al. [38], by drawing the Michaelis-Menten kinetic curve of the whole-cell biocatalyst and crude enzyme (Fig. S8a), the steady-state assumption is used to fit the linear relationship used to determine the effective diffusion coefficient (De) (Fig. S8b). The effective diffusion coefficient of the whole-cell biocatalyst E-22b-S was calculated to be 1.22 $\mu m^2/s$, which confirmed that the cell membrane has a diffusion barrier comparing the free diffusion coefficient of carbon dioxide in the water of 1940 $\mu m^2/s$. The use of surface display systems to construct a new type of whole-cell biocatalyst is a promising method to eliminate the cell membrane barrier. As mentioned above, the enzyme activity of the whole-cell biocatalyst E-22b-I_{RL}S was improved compared with that of E-22b-S. According to the Michaelis-Menten kinetic curve (Fig. S8a), the kinetic parameters of the whole-cell catalyst and crude enzyme were further determined. On the one hand, the k_{cat}/K_m reflecting the catalytic efficiency demonstrated that the whole-cell biocatalyst E-22b-I_{RL}S (4.55×10^4 1/M·s) was higher than that of E-22b-S (3.45×10^4 1/M·s) (Table S1). On the other hand, the K_m of E-22b-I_{RL}S is lower than E-22-S (Table S1), indicating that the surface display system improves the affinity of the enzyme and the substrate. Therefore, it can be inferred that applying the surface display system is feasible to eliminate the cell membrane barrier and improve catalytic efficiency. In prospective work aiming at improving the surface display efficiency of the whole-cell biocatalyst, the catalytic performance can be further enhanced.

Table 3
Effect of metal ions on the enzymatic activity of free SazCA and the E-22b-I_{RL}S whole-cell biocatalyst.

Metal ions	Concentration (mM)	Relative enzyme activity %	
		Free SazCA	E−22b-I_{RL}S
control	1.0	100 ± 1.70	100 ± 2.02
K^+	1.0	99.99 ± 3.45	88.13 ± 2.51
Na^+	1.0	80.20 ± 4.23	80.28 ± 2.89
Ca^{2+}	1.0	84.28 ± 2.30	84.12 ± 4.42
Mg^{2+}	1.0	85.78 ± 1.08	119.27 ± 1.79
Fe^{3+}	1.0	131.41 ± 6.32	159.11 ± 7.24
Li^+	1.0	13.74 ± 4.57	26.84 ± 3.53
Mn^{2+}	1.0	42.49 ± 3.42	74.22 ± 2.22
Cu^{2+}	1.0	5.29 ± 0.30	7.78 ± 1.30
Ni^{2+}	1.0	6.29 ± 2.79	18.23 ± 1.59
As^{3+}	1.0	6.56 ± 3.42	13.29 ± 2.34
Hg^{2+}	1.0	18.82 ± 2.08	17.00 ± 1.82
Pb^{2+}	1.0	71.24 ± 3.01	37.60 ± 2.75
Cd^{2+}	1.0	3.74 ± 2.23	10.28 ± 1.39
Zn^{2+}	0.5	75 ± 2.32	78 ± 3.77
Zn^{2+}	1.0	4.60 ± 1.22	5.15 ± 0.98
Zn^{2+}	1.5	0.32 ± 0.04	0.51 ± 0.03
Zn^{2+}	2.0	0 ± 0.02	0 ± 0.11

3.8. CO_2 mineralization

The surface display strain E-22b-I_{RL}S, free SazCA, and intracellular expression strain E-22b-S were tested in the actual CO_2 capture and mineralization process. The same mineralization system with the E-22b strain containing the empty plasmid pET22b was included as a negative control. The whole-cell biocatalyst and purified free SazCA were reported to effectively promote CO_2 hydration and convert CO_2 into $CaCO_3$ in the presence of use Ca^{2+} [52,53]. For a quick assessment, we compared the turbidity of E-22b-I_{RL}S, free SazCA, E-22b-S, and E−22b systems after adding $CaCl_2$ (Fig. S9). As expected, the mineralization system of the control group was clear and transparent, without apparent $CaCO_3$ precipitation. By contrast, the systems with E-22b-I_{RL}S, free SazCA, and E-22b-S quickly formed precipitates, whereby the mineralization system with E-22b-I_{RL}S and free SazCA was more turbid than that with E-22b-S. The system was maintained at 25 °C and reacted for 10 min. The amount of $CaCO_3$ produced by the different mineralization systems was directly weighed following suction filtration and drying (Fig. 7). Under the same conditions, the order of the amount of $CaCO_3$ produced by different mineralization systems was free SazCA (255 mg)> E-22b-I_{RL}S (241 mg)>E-22b-S (173 mg)>E-22b (88 mg). The amount of $CaCO_3$ produced by the surface display strain E-22b-I_{RL}S was significantly higher than that of the intracellular expression strain E-22b-S, indicating that SazCA was anchored on the cell's outer membrane. Neither the enzyme substrates nor enzymatic reaction products need to pass through the membrane barrier to directly contact the enzyme, reducing the mass transfer resistance of substrates and products and

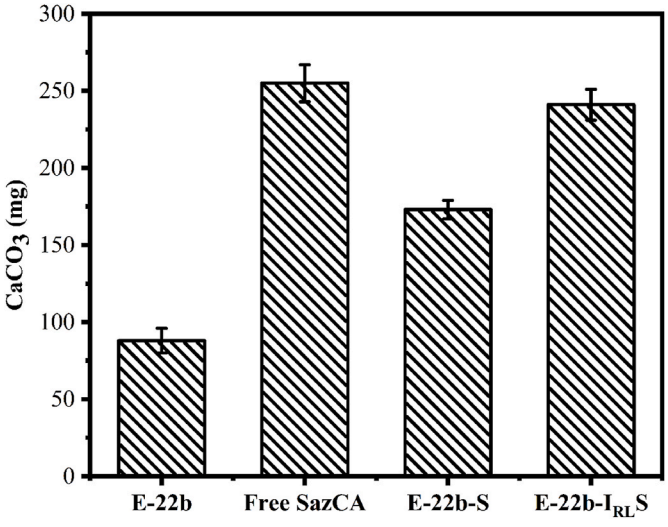

Fig. 7. $CaCO_3$ deposition in different mineralization systems.

increasing the whole-cell catalyst's enzyme activity, thus increasing the rate of $CaCO_3$ deposition.

4. Discussion

Reducing the emission of CO_2 into the atmosphere and converting it into useable materials is of great significance for sustainable development. As shown in Table 4, there have been few previous studies on the surface display of carbonic anhydrase. In the studies that have been reported, the whole-cell catalytic activity of the engineered surface display strains was not significant. At present, eight types of carbonic anhydrases that evolved independently have been reported, classified as α-, β-, γ-, δ-, ζ-, η-, θ-, and ι-CA [54]. Among them, the more common and more researched are the first two classes. To our knowledge, we demonstrated for the first time the display of α-carbonic anhydrase from *Sulfurihydrogenibium azorense* (SazCA) on the surface of *E. coli* cells to construct whole-cell biocatalysts. SazCA is different from γ-CA previously found in thermophilic bacteria, and it belongs to the α-CA class. In comparison with CA from *S. yellowstonense* YO3AOP1 (SspCA), *Helicobacter pylori* (hpαCA), the highly active human CA (hCA II), the human isoenzyme I (hCA I), and the bovine CA (bCA II), SazCA showed excellent stability and the highest catalytic efficiency of any CA reported to date [55]. We proved that surface display of SazCA on the surface of *E. coli* cells resulted in a significantly more powerful whole-cell biocatalyst than the surface display of HPCA. (Fig. 2). Considering the specificity of the CO_2 capture environment, as a highly efficient and thermostable biocatalyst, SazCA seems to be the best choice for CO_2 capture and mineralization.

INP is a secreted surface protein found in species of *Pseudomonas*, *Xanthomonas,* and *Erwinia* [56]. The expression system based on INP can achieve a higher surface display efficiency than the traditional prokaryotic surface display system based on Lpp-OmpA [57]. Fan et al. showed that the target protein displayed using INPN as a vector has the highest expression on a single cell, and the unit cell has the highest enzyme activity [30], which laid the foundation for our study. The successful construction of recombinant fusion proteins requires both a component protein and a connecting sequence. Selecting or rationally designing the protein fusion mode between the carrier protein and the target protein can greatly improve the folding stability of the fusion protein [15], promote protein expression, and enhance the biological activity of the displayed protein [12,58]. This study used the two front-end sub-repeats in the middle repeat domain of ice nucleoprotein and a flexible linker to connect INPN and CA, resulting in a fusion protein for cell surface display that maintains a distance between the carrier protein and the target protein (Fig. S10). The whole-cell catalytic activity of the surface display strain can be improved using this fusion pattern (Fig. 2). The intermediate repeat of ice nucleation protein (INP) is a highly versatile region, which can be used as an expandable linker to display target proteins at different distances from the cell surface [56,59]. This allows large fusion proteins to be displayed on the surface without interference from the surface of prokaryotic cells. The INP is the most stable and effective carrier for heterologous proteins, and it can be used to express cargoes of up to 60 kDa [60].

The fusion protein displayed on the cell surface is also fused with the PelB signal peptide encoded by the pET22b vector and the TrxA solubility tag encoded by the pET32a vector, respectively. In this study, the surface display system using the pET22b vector with the PelB signal peptide showed higher whole-cell enzyme activity (Fig. 2). Some auxiliary signal peptides such as PelB can be fused with the target protein to increase protein expression. However, the fusion of the solubility tag TrxA has not reported in previous studies to contribute to the efficient expression and correct folding of foreign proteins [61]. The expression of the fusion signal peptide PelB can be used to secrete the fusion protein into the extracellular space via the classical Sec pathway, which is beneficial for the formation of disulfide bonds while also avoiding hydrolysis by cytoplasmic proteases and the extension of *N*-terminal methionine [62]. Although the TrxA solubility tag can promote the correct folding of heterologous proteins [61,63], the whole-cell enzyme activity of strains expressing SazCA fused with TrxA was lower. One possible reason is that the surface area of a single cell is constant, and the smaller the protein displayed on the surface, the more can be displayed on the surface of each unit cell [26]. CA's catalytic activity in the whole cell was related to the displayed CA content and the steric hindrance of CA. However, the substrate of CA is CO_2, so that the steric hindrance can be disregarded. Thus, the whole-cell activity of the CA surface display strain was only related to the amount of CA displayed per cell. The higher the CA expression on a single cell's surface, the higher the overall enzyme activity of the biocatalyst. We can infer different fusion proteins have other effects on the target protein. Chaperones and folding enzymes should be selectively co-expressed according to the characteristics of the foreign protein. The fusion protein design should be optimized to display SazCA on the surface in future studies.

When using the SazCA cell surface display strain E-22b-I_{RL}S as a whole-cell biocatalyst in the CO_2 mineralization reaction, the amount of $CaCO_3$ produced by the E-22b-I_{RL}S system was slightly lower than that of the free SazCA (Fig. 7). The SazCA content in the same amount of whole-cell biocatalyst is theoretically lower than the same amount of free SazCA. We speculate that the more stable enzyme activity of SazCA on the cell surface results in E-22b-I_{RL}S and free SazCA exhibiting similar catalytic CO_2 hydration efficiency. Of course, whether it is E-22b-I_{RL}S or free SazCA, its active site is easier to contact with the substrate, so the catalytic efficiency is higher than that of E-22b-S. However, the thermal stability, pH stability, and long-term stability of free SazCA was significantly lower than that of SazCA displayed on the cell surface (Figs. 5 and 6), while also being much more expensive due to the need for protein purification. Moreover, free SazCA cannot be recycled and reused. By contrast, SazCA displayed on the cell surface can be separated, recovered, and reused by simple centrifugation or filtration. Therefore, cell surface display of SazCA has a number of advantages over free SazCA in industrial applications.

Enzyme immobilization is an effective way to stabilize the structure of the enzyme in industrial biocatalysis applications. To date, a variety

Table 4
Comparison of the activities of the whole-cell CA systems.

Host strain	Source of Carbonic Anhydrase	Enzyme activity[a]	References
E. coli BL21(DE3)	*Helicobacter pylori* (HPCA)	6.09×10^{-2} U·mL^{-1}OD$_{600}^{-1}$	Fan et al., 2011 [30]
E. coli BL21(DE3)	*Neisseria gonorrhoeae* (ngCA)	1.77 U·mL^{-1}OD$_{600}^{-1}$	Jo et al., 2013 [26]
S. cerevisiae	*Streptococcus thermophilus* (CAH)	2 U·nM^{-1}	Barbero et al., 2013 [31]
E. coli BL21(DE3)	*Helicobacter pylori* (HPCA)	3.0×10^{-2} U·mL^{-1}OD$_{600}^{-1}$	Watson et al., 2016 [32]
R. sphaeroides	*R. sphaeroides*	N.A.	Park et al., 2017 [34]
E. coli BL21(DE3)	*S. yellowstonense* (SspCA)	N.A.	Del Prete et al., 2017 [33]
E. coli BL21(DE3)	*Mesorhizobium loti* (MlCA)	83.54 U·mL^{-1}	Tan et al., 2018 [38]
E. coli BL21(DE3)	*Helicobacter pylori* (HPCA)	6.52×10^{-2} U·mL^{-1}OD$_{600}^{-1}$	This study
E. coli BL21(DE3)	*Sulfurihydrogenibium azorense* (SazCA)	11.43 U·mL^{-1}OD$_{600}^{-1}$	This study

[a] Values were calculated based on visible data of the original paper with standardized unit definition; N.A.: not available.

of immobilization strategies have been applied to CA with good properties, involving physical adsorption, covalent binding, encapsulation, and cross-linking [64]. Similar to the cell membrane, INPN, and fusion patterns in this work, the choice of support and immobilization method largely determine the catalytic activity and stability of CA, in addition to CA's structure and activity characteristics [65]. Generally, physical adsorption that CA is fixed on the support through weak interaction force can be used to improve the activity and stability of CA [66]. But the weak interaction force inevitably creates a potential separation between CA and support [67]. However, when a covalent bond is used between the CA and the support, it can be tightly bound and significantly improve the stability of CA [68]; but the changes involved in CA conformation also bring the possibility of CA denaturation and activity loss. Encapsulation can ensure that the spatial conformation of CA is not affected without interfering with the enzyme activity [69] but increase the barrier and the mass transfer resistance and decrease the catalytic efficiency of CA, unlike cell membrane. On the other hand, when CA is combined with a cross-linking agent to form a cross-linked enzyme without support, it shows good stability and reducd mass transfer resistance; but. it is still necessary to avoid enzyme inactivation and fragility in engineering applications.

In all, the favorable purpose of immobilized CA is to improve its stability while protecting the enzyme activity as much as possible, and the immobilized CA with some supports can be recycled and reused. However, if the immobilization method is not suitable, especially the diffusion restriction and steric hindrance caused by the introduction of the support, and the enzymatic properties of CA will inevitably be affected [64]. In this study, when SazCA is displayed on the host cell surface through INPN, the fusion protein and the outer cell membrane are covalently linked. Therefore, the surface-displayed SazCA has the advantages of the immobilized enzyme, and the covalent bonding site can be adjusted by genetic means. This immobilization method has little effect on the active site of the enzyme. Thus, SazCA displayed on the cell surface has the characteristics of immobilized enzymes, with more stable performance and high activity, while retaining the complete multi-enzyme system in the cell to realize enzyme cascade reactions. Crucially, displaying SazCA on the cell surface eliminates tedious purification and immobilization steps, equivalent to combining the three stages of enzyme preparation, purification, and immobilization into one step, making the practice more straightforward, and thereby greatly reducing the production cost. Therefore, the display of SazCA on the cell surface is more promising for industrial applications than conventional enzyme immobilization. However, the cell surface display CA technology is still in the laboratory research stage. The existing research on CA surface display systems mostly focused on exploring the molecular mechanism of fusion protein secretion and folding. In addition, some of the surface display hosts are conditional pathogens and non-food-grade strains, which should also be addressed in future studies.

5. Conclusions

INPN was used as the anchor protein to successfully display HPCA and SazCA on the surface of *E. coli* BL21(DE3). The surface display system with both the front two sub-repeats in the middle repeat domain of ice nucleoprotein and a linker in the fusion protein showed higher whole-cell enzyme activity. The whole-cell enzyme activity of the SazCA expression strain was significantly higher than that of the HPCA expression strain. The pET22b vector with the PelB signal peptide was more suitable for the surface display of HPCA and SazCA than pET28a and pET32a containing the TrxA solubility tag. The fusion protein was stably anchored on the surface of the outer cell membrane in the SazCA surface display system. Under the optimal induction conditions, the surface display strain showed the highest enzyme activity of SazCA reported to date (11.43 $U{\cdot}mL^{-1}OD_{600}{}^{-1}$) (Fig. 4), which was significantly higher than the whole-cell activity of the strain with intracellular expression of SazCA (8.355 $U{\cdot}mL^{-1}OD_{600}{}^{-1}$). The surface display of SazCA had little effect on cell growth, while the enzyme was more stable, and had a similar CO_2 mineralization effect as free SazCA. In conclusion, displaying SazCA on the cell surface through genetic engineering avoids the cell membrane barrier and improves the enzymatic activity of the whole-cell catalyst.

Ethics approval

This article does not contain any studies with human participants or animals performed by any of the authors.

Consent to participate

The authors agree to participate.

Consent for publication

The authors agree to submit the article.

CRediT authorship contribution statement

Yinzhuang Zhu: Validation, Formal analysis, Investigation, Data curation, Visualization, Writing – original draft, Writing – review & editing. **Yaru Liu:** Methodology, Investigation, Data curation, Writing – original draft. **Mingmei Ai:** Validation, Formal analysis. **Xiaoqiang Jia:** Conceptualization, Supervision, Data curation, Visualization, Funding acquisition, Writing – original draft, Writing – review & editing.

Declaration of competing interest

The authors declare that they have no known competing financial interests or personal relationships that could have appeared to influence the work reported in this paper.

Acknowledgements

The authors wish to acknowledge the financial support provided by the National Key Research and Development Program of China (Project No. 2018YFA0902100) and the National Natural Science Foundation of China (No. 22178262, No. 21576197).

Appendix A. Supplementary data

Supplementary data to this article can be found online at https://doi.org/10.1016/j.synbio.2021.11.008.

References

[1] Anderson TR, Hawkins E, Jones PD. CO_2, the greenhouse effect and global warming: from the pioneering work of Arrhenius and Callendar to today's Earth System Models. Endeavour 2016;40:178–87. https://doi.org/10.1016/j.endeavour.2016.07.002.

[2] Tan LS, Shariff AM, Lau KK, Bustam MA. Factors affecting CO_2 absorption efficiency in packed column: a review. J Ind Eng Chem 2012;18:1874–83. https://doi.org/10.1016/j.jiec.2012.05.013.

[3] Rogelj J, den Elzen M, Hoehne N, Fransen T, Fekete H, Winkler H, et al. Paris Agreement climate proposals need a boost to keep warming well below 2 °C. Nature 2016;534:631–9. https://doi.org/10.1038/nature18307.

[4] Zhou WG, Wang JH, Chen P, Ji CC, Kang QY, Lu B, et al. Bio-mitigation of carbon dioxide using microalgal systems: advances and perspectives. Renew Sustain Energy Rev 2017;76:1163–75. https://doi.org/10.1016/j.rser.2017.03.065.

[5] Cuesta AR, Song C. pH swing adsorption process for ambient carbon dioxide capture using activated carbon black adsorbents and immobilized carbonic anhydrase biocatalysts. ApEn 2020;280. https://doi.org/10.1016/j.apenergy.2020.116003.

[6] Feron PHM, Jansen AE. The production of carbon dioxide from flue gas by membrane gas absorption. Energy Convers Manag 1997;38:S93. https://doi.org/10.1016/S0196-8904(96)00252-X.

[7] Zhai T, Wang C, Gu F, Meng Z-h, Liu W, Wang Y. Dopamine/polyethylenimine-modified silica for enzyme immobilization and strengthening of enzymatic CO_2

conversion. ACS Sustainable Chem Eng 2020;8:15250–7. https://doi.org/10.1021/acssuschemeng.0c04975.
[8] Ben-Mansour R, Habib MA, Bamidele OE, Basha M, Qasem NAA, Peedikakkal A, et al. Carbon capture by physical adsorption: materials, experimental investigations and numerical modeling and simulations - a review. ApEn 2016;161:225–55. https://doi.org/10.1016/j.apenergy.2015.10.011.
[9] Sang Y, Huang J. Benzimidazole-based hyper-cross-linked poly(ionic liquid)s for efficient CO_2 capture and conversion. Chem Eng J 2020;385. https://doi.org/10.1016/j.cej.2019.123973.
[10] Song C, Liu Q, Ji N, Deng S, Zhao J, Li Y, et al. Alternative pathways for efficient CO_2 capture by hybrid processes-A review. Renew Sustain Energy Rev 2018;82:215–31. https://doi.org/10.1016/j.rser.2017.09.040.
[11] Olajire AA. CO_2 capture and separation technologies for end-of-pipe applications - a review. Energy 2010;35:2610–28. https://doi.org/10.1016/j.energy.2010.02.030.
[12] Kenarsari SD, Yang D, Jiang G, Zhang S, Wang J, Russell AG, et al. Review of recent advances in carbon dioxide separation and capture. RSC Adv 2013;3:22739–73. https://doi.org/10.1039/c3ra43965h.
[13] Agnew DE, Pfleger BF. Synthetic biology strategies for synthesizing polyhydroxyalkanoates from unrelated carbon sources. Chem Eng Sci 2013;103:58–67. https://doi.org/10.1016/j.ces.2012.12.023.
[14] Figueroa JD, Fout T, Plasynski S, McIlvried H, Srivastava RD. Advancesn in CO_2 capture technology - the US department of energy's carbon sequestration Program. Int J Greenhouse Gas Control 2008;2:9–20. https://doi.org/10.1016/s1750-5836(07)00094-1.
[15] Zheng H, Gao Z, Yin F, Ji X, Huang H. Effect of CO_2 supply conditions on lipid production of *Chlorella vulgaris* from enzymatic hydrolysates of lipid-extracted microalgal biomass residues. Bioresour Technol 2012;126:24–30. https://doi.org/10.1016/j.biortech.2012.09.048.
[16] Farrelly DJ, Everard CD, Fagan CC, McDonnell KP. Carbon sequestration and the role of biological carbon mitigation: a review. Renew Sustain Energy Rev 2013;21:712–27. https://doi.org/10.1016/j.rser.2012.12.038.
[17] Wong TS. Carbon dioxide capture and utilization using biological systems: opportunities and challenges. J Bioprocess Biotech 2014;4. https://doi.org/10.4172/2155-9821.1000155.
[18] Bhatia SK, Bhatia RK, Jeon J-M, Kumar G, Yang Y-H. Carbon dioxide capture and bioenergy production using biological system - a review. Renew Sustain Energy Rev 2019;110:143–58. https://doi.org/10.1016/j.rser.2019.04.070.
[19] Lindskog S. Structure and mechanism of carbonic anhydrase. Pharmacol Ther 1997;74:1–20. https://doi.org/10.1016/s0163-7258(96)00198-2.
[20] Liu Z, Bartlow P, Dilmore RM, Soong Y, Pan Z, Koepsel R, et al. Production, purification, and characterization of a fusion protein of carbonic anhydrase from *Neisseria gonorrhoeae* and cellulose binding domain from *Clostridium thermocellum*. Biotechnol Prog 2009;25:68–74. https://doi.org/10.1002/btpr.80.
[21] De Simone G, Di Fiore A, Capasso C, Supuran CT. The zinc coordination pattern in the η-carbonic anhydrase from *Plasmodium falciparum* is different from all other carbonic anhydrase genetic families. Bioorg Med Chem Lett 2015;25:1385–9. https://doi.org/10.1016/j.bmcl.2015.02.046.
[22] Wu Z, Nan Y, Zhao Y, Wang X, Huang S, Shi J. Immobilization of carbonic anhydrase for facilitated CO_2 capture and separation. Chin J Chem Eng 2020;28:2817–31. https://doi.org/10.1016/j.cjche.2020.06.002.
[23] Effendi SSW, Tan S-I, Ting W-W, Ng IS. Genetic design of co-expressed Mesorhizobium loti carbonic anhydrase and chaperone GroELS to enhancing carbon dioxide sequestration. Int J Biol Macromol 2021;167:326–34. https://doi.org/10.1016/j.ijbiomac.2020.11.189.
[24] Razzak A, Lee DW, Lee J, Hwang I. Overexpression and purification of gracilariopsis chorda carbonic anhydrase (GcCAα3) in *Nicotiana benthamiana*, and its immobilization and use in CO_2 hydration reactions. Front Plant Sci 2020;11. https://doi.org/10.3389/fpls.2020.563721.
[25] Jo BH, Moon H, Cha HJ. Engineering the genetic components of a whole-cell catalyst for improved enzymatic CO_2 capture and utilization. Biotechnol Bioeng 2020;117:39–48. https://doi.org/10.1002/bit.27175.
[26] Jo BH, Kim IG, Seo JH, Kang DG, Cha HJ. Engineered *Escherichia coli* with periplasmic carbonic anhydrase as a biocatalyst for CO_2 sequestration. Appl Environ Microbiol 2013;79:6697–705. https://doi.org/10.1128/aem.02400-13.
[27] Parmley SF, Smith GP. Filamentous fusion phage cloning vectors for the study of epitopes and design of vaccines. Adv Exp Med Biol 1989;251:215–8. https://doi.org/10.1007/978-1-4757-2046-4_21.
[28] Kacar B, Ge X, Sanyal S, Gaucher EA. Experimental evolution of *Escherichia coli* harboring an ancient translation protein. J Mol Evol 2017;84:69–84. https://doi.org/10.1007/s00239-017-9781-0.
[29] Schlegel S, Genevaux P, de Gier J-W. Isolating *Escherichia coli* strains for recombinant protein production. Cell Mol Life Sci 2017;74:891–908. https://doi.org/10.1007/s00018-016-2371-2.
[30] Fan L-H, Liu N, Yu M-R, Yang S-T, Chen H-L. Cell surface display of carbonic anhydrase on *Escherichia coli* using ice nucleation protein for CO_2 sequestration. Biotechnol Bioeng 2011;108:2853–64. https://doi.org/10.1002/bit.23251.
[31] Barbero R, Carnelli L, Simon A, Kao A, Monforte AD, Ricco M, et al. Engineered yeast for enhanced CO_2 mineralization. Energy Environ Sci 2013;6:660–74. https://doi.org/10.1039/C2EE24060B.
[32] Watson SK, Han Z, Su WW, Deshusses MA, Kan E. Carbon dioxide capture using *Escherichia coli* expressing carbonic anhydrase in a foam bioreactor. Environ Technol 2016;37:3186–92. https://doi.org/10.1080/09593330.2016.1181110.
[33] Del Prete S, Perfetto R, Rossi M, Alasmary FAS, Osman SM, AlOthman Z, et al. A one-step procedure for immobilising the thermostable carbonic anhydrase (SspCA) on the surface membrane of *Escherichia coli*. J Enzym Inhib Med Chem 2017;32:1120–8. https://doi.org/10.1080/14756366.2017.1355794.
[34] Park J-Y, Kim Y-H, Min J. CO_2 reduction and organic compounds production by photosynthetic bacteria with surface displayed carbonic anhydrase and inducible expression of phosphoenolpyruvate carboxylase. Enzym Microb Technol 2017;96:103–10. https://doi.org/10.1016/j.enzmictec.2016.10.005.
[35] Compostella ME, Berto P, Vallese F, Zanotti G. Structure of α-carbonic anhydrase from the human pathogen *Helicobacter pylori*. Acta Crystallographica Section F-Struc Biol Commun 2015;71:1005–11. https://doi.org/10.1107/s2053230x15010407.
[36] De Simone G, Monti SM, Alterio V, Buonanno M, De Luca V, Rossi M, et al. Crystal structure of the most catalytically effective carbonic anhydrase enzyme known, SazCA from the thermophilic bacterium *Sulfurihydrogenibium azorense*. Bioorg Med Chem Lett 2015;25:2002–6. https://doi.org/10.1016/j.bmcl.2015.02.068.
[37] Wilbur KM, Anderson NG. Electrometric and colorimetric determination of carbonic anhydrase. J Biol Chem 1948;176:147–54.
[38] Tan S-I, Han Y-L, Yu Y-J, Chiu C-Y, Chang Y-K, Ouyang S, et al. Efficient carbon dioxide sequestration by using recombinant carbonic anhydrase. Process Biochem 2018;73:38–46. https://doi.org/10.1016/j.procbio.2018.08.017.
[39] Baneyx F, Mujacic M. Recombinant protein folding and misfolding in *Escherichia coli*. Nat Biotechnol 2004;22:1399–408. https://doi.org/10.1038/nbt1029.
[40] Ramanan R, Kannan K, Sivanesan SD, Mudliar S, Kaur S, Tripathi AK, et al. Bio-sequestration of carbon dioxide using carbonic anhydrase enzyme purified from *Citrobacter freundii*. World J Microbiol Biotechnol 2009;25:981–7. https://doi.org/10.1007/s11274-009-9975-8.
[41] Khalid A, Tayyab M, Hashmi AS, Yaqub T, Awan AR, Wasim M, et al. Optimization of conditions for maximal production of recombinant thermostable cellulase from *Thermotoga naphthophila* using *E. coli* BL21-CodonPlus (DE3) as expression host. Pakistan J Zool 2019;51:1371–7. https://doi.org/10.17582/journal.pjz/2019.51.4.1371.1377.
[42] Bose H, Satyanarayana T. Microbial carbonic anhydrases in biomimetic carbon sequestration for mitigating global warming: prospects and perspectives. Front Microbiol 2017;8. https://doi.org/10.3389/fmicb.2017.01615.
[43] Kumar S, Deshpande PA. Structural and thermodynamic analysis of factors governing the stability and thermal folding/unfolding of SazCA. PLoS One 2021;16. https://doi.org/10.1371/journal.pone.0249866.
[44] Chen YP, Hwang IE, Lin CJ, Wang HJ, Tseng CP. Enhancing the stability of xylanase from *Cellulomonas fimi* by cell-surface display on *Escherichia coli*. J Appl Microbiol 2012;112:455–63. https://doi.org/10.1111/j.1365-2672.2012.05232.x.
[45] Zhang Y, Dong W, Lv Z, Liu J, Zhang W, Zhou J, et al. Surface display of bacterial laccase CotA on *Escherichia coli* cells and its application in industrial dye decolorization. Mol Biotechnol 2018;60:681–9. https://doi.org/10.1007/s12033-018-0103-6.
[46] Ezemaduka AN, Yu J, Shi X, Zhang K, Yin C-C, Fu X, et al. A small heat shock protein enables *Escherichia coli* to grow at a lethal temperature of 50 °C conceivably by maintaining cell envelope integrity. J Bacteriol 2014;196:2004–11. https://doi.org/10.1128/jb.01473-14.
[47] Schutz MK, Lopes NF, Cenci A, Ketzer JMM, Einloft S, Dullius J, et al. Influence of alkaline additives and buffers on mineral trapping of CO_2 under mild conditions. Chem Eng Technol 2018;41:573–9. https://doi.org/10.1002/ceat.201600513.
[48] Jonsson BM, Hakansson K, Liljas A. The structure of human carbonic anhydrase II in complex with bromide and azide. FEBS Lett 1993;322:186–90. https://doi.org/10.1016/0014-5793(93)81565-h.
[49] Ferry JG. The γ class of carbonic anhydrases. Biochim Biophys Acta Protein Proteonomics 2010;1804:374–81. https://doi.org/10.1016/j.bbapap.2009.08.026.
[50] Maguire J, Watkin N. Carbonic anhydrase inhibition. Bull Environ Contam Toxicol 1975;13:625–9. https://doi.org/10.1007/bf01685190.
[51] Riordan JF. The role of metals in enzyme activity. Ann Clin Lab Sci 1977;7:119–29.
[52] Kim IG, Jo BH, Kang DG, Kim CS, Choi YS, Cha HJ. Biomineralization-based conversion of carbon dioxide to calcium carbonate using recombinant carbonic anhydrase. Chemosphere 2012;87:1091–6. https://doi.org/10.1016/j.chemosphere.2012.02.003.
[53] Sundaram S, Thakur IS. Induction of calcite precipitation through heightened production of extracellular carbonic anhydrase by CO_2 sequestering bacteria. Bioresour Technol 2018;253:368–71. https://doi.org/10.1016/j.biortech.2018.01.081.
[54] Alissa SA, Alghulikah HA, Alothman ZA, Osman SM, Del Prete S, Capasso C, et al. Inhibition survey with phenolic compounds against the δ- and η-class carbonic anhydrases from the marine diatom *thalassiosira weissflogii* and protozoan *Plasmodium falciparum*. J Enzym Inhib Med Chem 2020;35:377–82. https://doi.org/10.1080/14756366.2019.1706089.
[55] De Luca V, Vullo D, Scozzafava A, Carginale V, Rossi M, Supuran CT, et al. An α-carbonic anhydrase from the thermophilic bacterium *Sulphurihydrogenibium azorense* is the fastest enzyme known for the CO_2 hydration reaction. Biorg Med Chem 2013;21:1465–9. https://doi.org/10.1016/j.bmc.2012.09.047.
[56] Li L, Kang DG, Cha HJ. Functional display of foreign protein on surface of *Escherichia coli* using N-terminal domain of ice nucleation protein. Biotechnol Bioeng 2004;85:214–21. https://doi.org/10.1002/bit.10892.
[57] Karami A, Latifi AM, Khodi S. Comparison of the organophosphorus hydrolase surface display using InaVN and lpp-OmpA systems in *Escherichia coli*. J Microbiol Biotechnol 2014;24:379–85. https://doi.org/10.4014/jmb.1309.09066.
[58] Jia X, Li Y, Xu T, Wu K. Display of lead-binding proteins on *Escherichia coli* surface for lead bioremediation. Biotechnol Bioeng 2020;117:3820–34. https://doi.org/10.1002/bit.27525.

[59] Jung HC, Lebeault JM, Pan JG. Surface display of Zymomonas mobilis levansucrase by using the ice-nucleation protein of *Pseudomonas syringae*. Nat Biotechnol 1998; 16:576–80. https://doi.org/10.1038/nbt0698-576.

[60] Lee SY, Choi JH, Xu ZH. Microbial cell-surface display. Trends Biotechnol 2003;21: 45–52. https://doi.org/10.1016/s0167-7799(02)00006-9.

[61] LaVallie ER, DiBlasio EA, Kovacic S, Grant KL, Schendel PF, McCoy JM. A thioredoxin gene fusion expression system that circumvents inclusion body formation in the *E. coli* cytoplasm. Biotechnology 1993;11:187–93. https://doi.org/10.1038/nbt0293-187.

[62] Mergulhao FJM, Summers DK, Monteiro GA. Recombinant protein secretion in *Escherichia coli*. Biotechnol Adv 2005;23:177–202. https://doi.org/10.1016/j.biotechadv.2004.11.003.

[63] Hawkins HC, Blackburn EC, Freedman RB. Comparison of the activities of protein disulphide-isomerase and thioredoxin in catalysing disulphide isomerization in a protein substrate. Biochem J 1991;275(Pt 2):349–53. https://doi.org/10.1042/bj2750349.

[64] Ren SZ, Chen RX, Wu ZF, Su S, Hou JX, Yuan YL. Enzymatic characteristics of immobilized carbonic anhydrase and its applications in CO_2 conversion. Colloids Surf B Biointerfaces 2021:204. https://doi.org/10.1016/j.colsurfb.2021.111779.

[65] Yushkova ED, Nazarova EA, Matyuhina AV, Noskova AO, Shavronskaya DO, Vinogradov VV, et al. Application of immobilized enzymes in food industry. J Agric Food Chem 2019;67:11553–67. https://doi.org/10.1021/acs.jafc.9b04385.

[66] Lv B, Yang Z, Pan F, Zhou Z, Jing G. Immobilization of carbonic anhydrase on carboxyl-functionalized ferroferric oxide for CO_2 capture. Int J Biol Macromol 2015;79:719–25. https://doi.org/10.1016/j.ijbiomac.2015.05.051.

[67] Shi J, Wu D, Zhang L, Simmons BA, Singh S, Yang B, et al. Dynamic changes of substrate reactivity and enzyme adsorption on partially hydrolyzed cellulose. Biotechnol Bioeng 2017;114:503–15. https://doi.org/10.1002/bit.26180.

[68] Bhattacharya S, Schiavone M, Chakrabarti S, Bhattacharya SK. CO_2 hydration by immobilized carbonic anhydrase. Biotechnol Appl Biochem 2003;38:111–7. https://doi.org/10.1042/ba20030060.

[69] Yadav RR, Mudliar SN, Shekh AY, Fulke AB, Devi SS, Krishnamurthi K, et al. Immobilization of carbonic anhydrase in alginate and its influence on transformation of CO_2 to calcite. Process Biochem 2012;47:585–90. https://doi.org/10.1016/j.procbio.2011.12.017.